A molecular dynamics study of water chain formation in the proton-conducting K channel of cytochrome c oxidase

R.I. Cukier*

Department of Chemistry, Michigan State University, East Lansing, MI 48824-1322, United States

Abstract

The formation of water chains in cytochrome c oxidase (CcO) is studied by molecular dynamics (MD). Focus is on water chains in the K channel that can supply a proton to the binuclear center (the heme a_3 Fe/Cu_B region), the site of O_2 reduction. By assessing the presence of chains of any length on a short time scale (0.1 ps), a view of the kinds of chains and their persistence is obtained. Chains from the entry of the channel on the inner membrane to Thr359 (*Rhodobacter sphaeroides* numbering) are often present but are blocked at that point until a rotation of the Thr359 side chain occurs, permitting formation of chains from Thr359 towards the binuclear center. No continuous hydrogen-bonded water chains are found connecting Thr359 and the binuclear center. Instead, waters hydrogen bond from Thr359 to the hydroxyl of the heme a_3 farnesyl and then continue to the binuclear center via Tyr288, which has been identified as a source of a proton for O_2 reduction. Three hydrogen-bonded waters are found to be present in the binuclear center after a sufficiently long simulation time. One is ligated to the Cu_B and could be associated with a water (or hydroxyl) identified in the crystal structure as the fourth ligand of Cu_B. The water hydrogen-bonded to the hydroxyl of Tyr288 is extremely persistent and well positioned to participate in O_2 reduction. The third water is located where O_2 is often suggested to reside in mechanistic studies of O_2 reduction.
© 2004 Elsevier B.V. All rights reserved.

Keywords: Cytochrome c oxidase; Proton transfer and translocation; Molecular dynamics

1. Introduction

Cytochrome c oxidase (CcO) is an integral membrane protein that catalyzes the reduction of oxygen to water while producing a proton electrochemical gradient across the membrane that is ultimately used for ATP synthesis. The details of this process are quite complex, involving electron and proton transfer reactions and the translocation of protons across the membrane [1–8]. The mechanism of proton transfer and translocation through channels in CcO is thought to be governed by waters that are hydrogen-bonded to each other and to residues. Proton translocation may occur via chains of hydrogen-bonded waters, using a "proton wire" concept [9] that has its origin in the Grotthuss

[10] mechanism. The speed of transport is attributed to an excess proton "hopping" along the water chain by a series of making and breaking hydrogen bonds, which does not require the slow process of molecular diffusion.

One channel for proton transport in CcO has been termed the K channel because of a conserved Lysine (Lys362, in the numbering scheme for *Rhodobacter sphaeroides*) in its pathway (see Fig. 1) [11,12]. It connects the inner membrane around Ser299 to the binuclear center that is formed from two of the four redox active metals, Fe(II/III) in heme a_3 and a nearby Cu(I/II), designated as Cu_B. The heme a_3 Cu_B binuclear site is the catalytic heart of the enzyme where bound O_2 is reduced to H_2O with the use of at least one proton delivered through the K channel. The K pathway has Thr359 as a potential polar group for hydrogen bonding water to aid in proton translocation. The Lys362 side chain has been suggested to be a rotatable group dependent on its protonation state and thus involved in

* Tel.: +1 517 355 9715; fax: +1 517 353 1793.
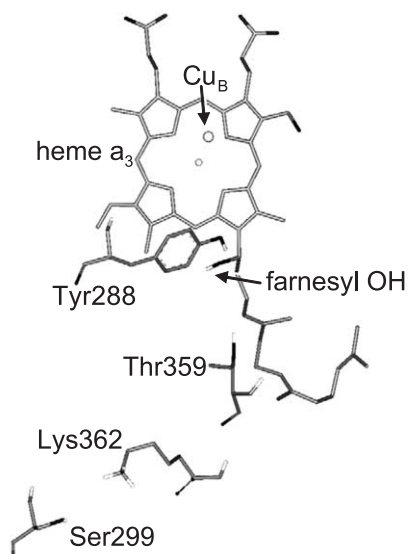*E-mail address:* cukier@cem.msu.edu.

Fig. 1. The K-pathway, in *R. sphaeroides* numbering, that can conduct a proton to the binuclear center formed by the heme a_3 Fe and Cu_B. The K-pathway entrance may be Ser299, near the inner membrane surface, and connects to the binuclear center via waters hydrogen-bonded to each other and to the intervening residues Lys362, Thr359 and Tyr288 and the hydroxyl of the heme a_3 farnesyl.

proton translocation [13]. A tyrosine (Tyr288) that is close to the binuclear center and cross-linked to His284 is thought to play an important role in the catalysis [14–16]. Another entry point for the K channel has recently been suggested to be Glu101 in subunit II [17,18]. We do not consider this entry point in our simulations for reasons discussed in Results. This definition of the K channel merges with the one we use at Lys362 and, since the impediments to and mechanisms for water chain formation and proton translocation arise in the region from Lys362 to the binuclear center, the definition used here is still appropriate.

In this work we use molecular dynamics (MD) to study the formation and properties of water chains in the K channel of CcO. The simulation is based on our previous work that examined, by a combination of quantum mechanics for proton transfer and classical mechanics (MD) for heavy atoms, proton transfer in CcO [19,20]. The role of waters that hydrogen bond to Glu286, once protonated, to in turn protonate Glu286, was addressed by these methods. In our simulation methodology, the protein atoms and a large number of solvent waters are completely free to move under the influence of the Newtonian forces. In MD simulations, waters are included by introducing the protein to a solvated box, and then excluding waters that overlap the protein. Proceeding this way will rely on a slow, electrostatically guided diffusion process to populate the protein with water. Therefore, in addition to these waters, waters are added to the protein interior by a search algorithm designed to find suitable locations. Then, water chains are more likely to form on the MD time scale. Chains of hydrogen-bonded waters/ residues may be quite transient in nature, especially as they

become long, other things being equal. Yet, because of the potential speed of proton translocation, they do not have to be in existence for very long to be effective. Since the MD time scale is intrinsically short, the ability to capture rare events can be a key to success in these studies. Thus, it is important to be able to interrogate the formation of chains frequently and to be able to identify them when they occur. To address the former issue, we collect water coordinate data on a 0.1-ps time scale for waters within what will be defined as the K channel. Note that it would be impractical to collect all (approximately 20,000) water coordinates on a 0.1-ps time scale. The latter issue was solved with the use of a program that constructs "trees" of hydrogen-bonded water molecules [21]. In principle, the donor/ acceptor hydrogen bonding property of water will produce, from a root water, a ramifying tree of hydrogen-bonded waters; though, within the confines of a protein, such trees are expected to be severely pruned. Another feature that is important to investigate is the stability of waters that are hydrogen bonding to each other and/or to residues. We will consider the persistence of waters around residues to locate those where one or more waters may play a decisive mechanistic role.

The other prominent channel that leads from the inner membrane (around Asp132) to Glu286 is known as the D channel [14,22–24]. Crystallographic studies [12,14,15] reveal a chain of hydrogen-bonded water molecules in this channel, supporting the concept of hydrogen-bonded water/residues as supporting proton translocation. In contrast, the K channel is found to have few waters [12,18] and then a quandary that arises is the elucidation of pathways for proton conduction. It proved convenient for our analysis to consider three regions of the K pathway that have distinct characteristics. First is the region Ser299–Lys362–Thr359. We find that water chains are readily formed in this region and that it is possible to "skip" Lys362 and suggest that it is Thr359 that may act as a switch point for proton translocation. That is, there may be a rotation of the Thr359 side chain required to connect water chains from Ser299 to Thr359 and from Thr359 to Tyr288. The importance of Thr359 to enzyme activity has been demonstrated by the drastic drop in activity upon its mutation to alanine [25]. Second is the region Thr359–Tyr288. It is a very hydrophobic region and it is difficult to rationalize support for proton transport here. What the simulation reveals is a key role for the hydroxyl of the heme a_3 farnesyl in providing a hydrogen-bonded water chain that connects Thr359 to Tyr288. The involvement of the farnesyl hydroxyl in helping provide a proton to the binuclear center was suggested previously on the basis of quantum chemical investigations [26]. Third is the region from Tyr288 to the binuclear center. Here, we will find that specific waters are hydrogen-bonded to residues and within interaction distance of the heme a_3 Fe and Cu_B in a way that could provide protons to facilitate oxygen reduction.

A number of informative simulations of CcO have been carried out before [13,27–33], which have addressed issues such as Glu286 acting as a proton shuttle [19,20,27,28], the formation of water chains [13,19,20,29,30,33] and the coupling between proton transfer and enzyme redox state. [30–32]. Distinguishing features of our MD simulation are the use of a large number of explicitly treated solvating waters that evolve under their mutual and protein inter-actions (no positional restraints), and the methodologies used to analyze water chain formation.

2. Computational methodology

2.1. Molecular dynamics

The MD simulations were carried out using CUKMODY, a code designed for the efficient simulation of proteins and other large solutes [21]. The GROMOS force field [34] was used for the residues and water. The additions to the force field required to simulate CcO are discussed below. A combination of a cell index method with linked lists [35] and a Verlet neighbor list [36] is used to provide linear scaling with the number of atoms in the pair list routine. The electrostatic interactions are evaluated using the charge-group method, to be consistent with the parameterization of the GROMOS force field. Periodic boundary conditions are used. The SHAKE algorithm [37] is used to constrain bond lengths permitting a 2-fs time step. The simulation is carried out at constant NVT with velocity scaling to control the temperature to around 300 K [38]. The start-up protocol creates a face-centered cubic lattice of water molecules and centers the protein in the simulation cell, and waters that overlap the protein are discarded. The simulation is started with the protein cold, and the solvent heats the protein as the solvent molecules equilibrate to each other and the protein.

The initial configuration for MD is a preliminary version [39] of the recently published X-ray crystal structure of CcO from *R. sphaeroides* [12]. Subunits I and II and the polar hydrogens that were added by use of the MOE program (Chemical Computing Group, Inc.: http://www.chemcomp. com/) along with 18,399 water molecules left in the simulation box, after eliminating overlapping waters, were simulated. The box side is 88.7 Å, and the largest dimension of CcO is around 80 Å, leaving about 20 Å between protein molecules in neighboring cells. The large number of waters used facilitates investigation of the formation of hydrogen-bonded water structures.

The histidine residues are assumed neutral (singly protonated), the aspartic and glutamic acids are ionized (−1), and the lysines and arginines are protonated (+1). A force field for the two heme a's (with their farnesyl "tails") was constructed based on the GROMOS force field's heme *c*. Both heme groups are assumed to be in their reduced states, with formal charge Fe^{2+}. The Cu_B, also assumed reduced (+1), is ligated to three histidine residues (His284,

His333, His334). With charge delocalization to these histidines, the MD charge of Cu_B is assigned as +0.41, a value essentially the same as used in Hofacker and Schulten's CcO study [13]. The Tyr288 ring C6 and His244 NE (ϵ nitrogen on the imidazole ring) atoms are covalently linked, in accord with crystallographic results [12]. The Cu_A–Cu_A site forms a I–II mixed valence compound (Robin-Day type III) leading to formal charges of +1.5 per Cu_A [40]. One Cu_A is ligated to Glu254, Cys256, and His260, and the other to His217, Cys252 and Met264. For MD purposes, the charges are assigned as +0.75 per Cu_A, because of the charge transfer to the (deprotonated) cysteine ligands. The two His ligands are assigned +0.25 charge and each of the two (deprotonated) cysteine ligands a total charge of −0.5 [13]. The magnesium and calcium ions are assigned their formal charges of +2.

2.2. Water insertion

The elimination of waters that overlap protein atoms may leave space for additional waters within the protein. Space for additional interior waters was found by first scanning a van der Waals test sphere, with water's σ value, over a grid with spacing of 1.5 Å in each of the three Cartesian coordinate directions. If the total van der Waals interaction with neighboring atoms is less than 2 kcal/mol, this test sphere becomes a candidate test sphere. Each such candidate is made into a test water (TW) by inserting water's electrostatic charges and the candidate is "spun" over a set of 18 orientations, the energy evaluated for each orientation, and the minimum energy one accepted. Carrying out this procedure for all candidates and accepting all whose energy lie below −2 kcal/mol provides a refined set of TWs. (Different choices for the energetic cutoffs lead to similar results, as long as the van der Waals energy is not chosen as very large or the electrostatic energy as very negative.) The energetic cutoff just serves as an aid to place waters at potentially favorable positions. Once the simulation starts, they energetically stabilize by finding more suitable locations, inside the protein or in the bulk solvent, and by reorganizing the surrounding medium. Some of these waters were close to each other, because of the 1.5-Å grid spacing that we used. For those that are closer than a hydrogen-bonding distance (oxygen–oxygen distance less than 2.7 Å), one of the pair was eliminated. This algorithm was used to insert approximately 500 more waters into the protein, and they are included in the MD simulation.

2.3. Channel definition and water chain algorithm

The K channel definition adopted here has Ser299 as a potential entrance point and Cu_B as a termination point. To provide a viable method of searching for water structures that can span either completely or in part(s) this region, and do so on a fine grain in time, we define a K channel as all waters that are found in a cylinder of radius 10 Å whose axis

spans the Ser299 OH and Cu_B. As the MD proceeds, the coordinates of all waters within the K channel are saved every 0.1 ps. With this frequent interrogation of water configurations, we can assess the statistics of chain formation/destruction and the identification of "rare" configurations. It should be appreciated that within the intrinsically short MD simulation time scale, especially for a large protein with a large number of solvating waters that requires a great deal of processing time for the simulation, rare configurations are not easy to capture.

A program we developed to construct hydrogen-bonded water "trees" was then used to identify interesting water/protein structures in this cylinder [21]. To construct a tree, first a "root" water is picked. All waters (level 1) that are hydrogen-bonded to the root (level 0) are stored, and the root removed from the list of possible hydrogen bond formers. Each level 1 water is, in turn, considered as a root and all waters hydrogen-bonded to each of these are stored (level 2), and all level 1 waters removed from the list of possible hydrogen bond formers, and this procedure is continued recursively. Picking a desired number of levels, N_{lev}, will then produce, for all the MD steps considered, all trees of hydrogen-bonded waters of at least length N_{lev}. A terminal water can also be specified, leading to the identification of water trees with given origin and termination points. The criterion for hydrogen bond formation can be varied from, for examples, "easy" where all members of a tree have Oa–Ob distance d_{OaOb} between the oxygens of waters a and b $d_{OaOb} < 3.5$ Å to "severe", $d_{OaOb} < 3.0$ Å, and the OaHOb angle A_{OaHOb} $180° < A_{OaHOb} < 145°$.

2.4. Persistent waters algorithm

Most of the waters that are displayed in the figures we generate are eventually replaced by other waters, though some (that we shall note at the appropriate places) are quite persistent. Clearly, the persistence time requires an operational definition. We define it to be on the order of 100 ps since on this time scale, if we are interested in excess proton conduction along a hydrogen-bonded chain, many protonic jumps can occur (an excess proton can hop back and forth between water and/or residue heavy atoms many times [19,20]), yet the time is long enough that at least locally the protein can respond to the new charge distribution that exists after a particular proton transfer event and rearrange to accommodate the new charge distribution. For a given hydrogen-bonded structure, where there is a water chain connecting two residues, at some other close-by instant of time the chain may be broken in one or more places, and shortly thereafter it may reform. Thus, while we provide snapshots of chains, it should be evident that they are forming and reforming dynamically. Of course, for a given data set, the percentage of complete chains will also depend on the definition of a hydrogen bond.

Waters that are persistent should correspond to relatively low-energy configurations. Thus, it is also of interest to evaluate the solvation energies of persistent waters, which includes their interaction with other waters, residue atoms, the hemes and the metals. The energy will fluctuate with MD step and it should be noted that the absolute value is not a precise number, since such values depend on the particulars of the force field and the cutoff radius used to evaluate the energy. Of use, though, is to compare the energies of waters that are inside the protein with the average solvation energy of water with itself, the pure solvent. This latter solvation energy is approximately −18 kcal/mol with a root mean square deviation from the mean of approximately 2 kcal/mol. Of course, thermodynamic stability can only be assessed by evaluating a free energy, and that is beyond the scope of these simulations.

3. Results

The distance between Ser299 and Cu_B (Fig. 1) in the *R. sphaeroides* [12] structure is approximately 24 Å. For purposes of orientation, the distances between a number of atoms are: Ser299 CA-(9.4 Å)-Lys362 CA-(5.1 Å)-Thr359 CA-(7.1 Å)-heme a_3 farnesyl O1B-(2.9 Å)-Tyr288 OH-(5.8 Å)-Fe, where O1B denotes the farnesyl oxygen and OH denotes the tyrosine's hydroxyl oxygen. The Fe–Cu_B distance is 4.6 Å. Over the 3 ns of simulation time, most of the protein structure is well preserved. The alpha-helical bundles that would span the membrane are stable over the simulation with one exception. In the interface between subunits I and II, around Glu101 of subunit II, a possible K-pathway channel entrance [18], there is some loss of structure. Thus, we cannot safely analyze water chain formation from this other potential entrance of the K channel. However, there should be no difficulty in water chain formation from Glu101 to the vicinity of Lys362 since this region is very solvent-accessible. The discussion of the simulation results is divided into three parts, corresponding to three regions of the K-channel that have distinct properties.

3.1. Ser299–Lys362–Thr359

The geometry of the three residues, Ser299, Lys362 and Thr359 is well preserved during the entire MD run, as shown by the data in Table 1 that lists Ser299 CA–Lys362 CA and Lys362 CA–Thr359 CA distances for several times

Table 1
Distances between atoms of selected residues for several MD times

Time (ns)	0.0[a]	1.5	3.0
Ser299 CA[b]–Lys362 CA (Å)	9.4	8.9	9.6
Lys362 CA[b]–Thr359 CA (Å)	5.1	5.4	5.3
Ser299 CA[b]–Lys362 NZ[b] (Å)	7.0	6.6	6.2
Lys362 NZ[b]–Thr359 CA (Å)	7.8	8.1	8.5

[a] Crystal structure.
[b] CA is the alpha carbon. NZ is the amino group nitrogen.

during the 3-ns run. The small fluctuations in these distances provide a stable framework within which to view the formation of hydrogen-bonded water/residue structures. The panels of Figs. 2 and 3 show snapshots of waters hydrogen-bonded to residues and/or to other waters. These snapshots are separated in time by 50 ps and were captured around 3 ns after startup. The hydrogen bond search algorithm discussed in Computational methodology analyzes the K channel data every 0.1 ps and permits the conclusion that Figs. 2 and 3 are representative of the generated data. However, we should stress that the pattern of Fig. 3 is more common than that of Fig. 2. Also, the chains do form, then break up and reform, and may involve other waters than those displayed in the figures.

Fig. 2 shows a direct water chain Ser299–W8827–W4434–W1359–W18680–Thr359 spanning Ser299 to Thr359 that bypasses Lys362, indicating that there are ways to conduct protons without direct involvement of Lys362. The short lengths of the hydrogen bonds spanning Ser299 to Thr359 show that they are strong. This suggests the possibility of Thr359 as the key residue for this part of the pathway, as an alternative to K362. On the other hand, Fig. 3 shows that the chain to Thr359 can be disrupted. Analysis of a number of snapshots shows that the disruption is most likely a consequence of the rotation of the Thr359 hydroxyl to point further up, in the view of Figs. 2 and 3. The rotation of the Thr359 hydroxyl introduces the possibility of Thr359 being a switch point for proton conduction in this part of the K pathway.

Fig. 3. The residues Ser299 and Lys362 are connected by W8827 (larger view), but there is no direct chain to Thr359 as in Fig. 2. The W8827 bridging Ser299 and Lys362 is quite persistent. The Thr359 hydroxyl appears to have rotated somewhat higher relative to its position in Fig. 2 and this may be responsible for disrupting the direct chain from Ser299 to Thr359.

The W8827 that is present in Figs. 2 and 3 bridges the Ser299 hydroxyl and the Lys362 amino group. It is persistent in the sense that over the 100-ps time interval after the snapshot of Fig. 2, the maximum displacement of W8827 is 1.7 Å. That is, the magnitude of this water's largest minus smallest distance relative to the protein's center of mass is 1.7 Å. The average energy of solvation for this water, −18 kcal/mol, is given in Table 2 along with solvation energies of other waters, and is comparable to the solvation energy of water in water (also −18 kcal/mol). For the 100 ps before the data displayed in Fig. 2, W8827 is still hydrogen-bonded to Lys362. However, looking at data 1.5 ns before the data presented here, while there is a similar persistently hydrogen-bonded water to Lys362, it is not W8827. Around 1.2 ns W10198 becomes hydrogen-bonded to Lys362 and remains so until around 2 ns. Then, W8827 exchanges with W10198 and becomes hydrogen-bonded to Lys362 for remaining simulation duration of 3 ns. Thus, at any given time after about 1 ns into the simulation, a water bridges Lys362 and Ser299 and does so with about 1-ns persistence time.

There are other waters that hydrogen bond to Lys362 and, on average, Lys362 is hydrogen bonding to three waters. Some of these waters are more and others less stable than W8827 in terms of their maximum excursion relative to the protein's center of mass, over a given time interval, and eight different waters are involved in hydrogen bonding to Lys362 over the 200-ps interval examined here. Thus, we may conclude that Lys362 is well "solvated" by hydrogen-bonded waters. This Lys362 solvation then argues that it should be considered as protonated at normal pH, in support of the experimental conclusions [41].
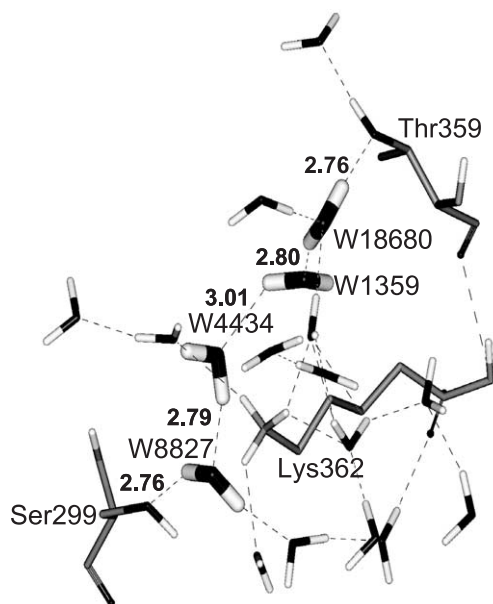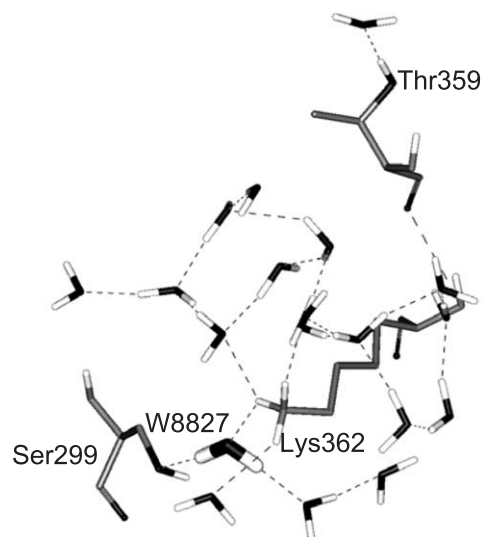

Fig. 2. The residues Ser299 and Thr359 are connected by a hydrogen-bonded chain of four waters (displayed in larger view). The hydrogen bonding distances are indicated (in Å), and show that these are all strong hydrogen bonds. The other hydrogen-bonded waters in this region of the K channel are also displayed (displayed in smaller view).

Table 2
Solvation energies of selected persistent waters

Water	Solvent[a]	18 668[b,c]	18 402[b]	5005[b]	8827[d]	18 680[d]
Energy (kcal/mol)	−18.0	−20.0	−30.0	−16.0	−18.0	−15.0

[a] A water in solvent water in this simulation.
[b] See Fig. 9.
[c] See Fig. 7.
[d] See Fig. 2.

The data in Table 1 listing the Ser299 CA–Lys362 NZ and Lys362 NZ–Thr359 CA distances (CA is an alpha carbon and NZ is the lysine amino group nitrogen) serve to show that Lys362 is not undergoing a large side chain movement. Indeed, over the 3-ns time interval, these distances fluctuate roughly on the same scale as the corresponding CA to CA distances. An examination of snapshots visualized in three dimensions also shows that there is little lysine side chain movement. Thus, our simulation, which assumes that Lys362 is protonated, does not exhibit a movement to support it being a pivot point for a proton relay.

Examination of the persistence of waters hydrogen-bonded to Thr359 shows that water is fluxional here and that the orientation of the residue side chain is important in whether a water below or above the Thr359 is hydrogen bonding. In Fig. 2, there are two hydrogen-bonded waters to Thr359. In Fig. 3, there is one hydrogen-bonded water above and in other configurations there are none. The above-the-Thr359 hydrogen-bonded water configuration can persist for order 100 ps. These features show that the rotation of the Thr359 side chain is crucial in making and breaking the chain from Ser299.

The possible role of the hydroxyl group of Thr359 as a "pivot" point that can connect to Ser299 when it is pointing down (in the orientation of Figs. 2 and 3) and eventually to Tyr288 when it is pointing up is illustrated in stereo-view in Fig. 4. Before rotation (left-lower part of the figure), the hydroxyl group points down, after rotation it points up (right-higher part of the figure). When it is pointing down, there are water chains connecting to Ser299. When the

Thr359 rotates its hydroxyl group toward the top, then, as far as we can tell from our data, these chains cannot exist because the hydroxyl is now ill-positioned. After rotation, the hydroxyl group is now positioned to hydrogen bond to waters that can continue upward to eventually connect with Tyr288. Thus, we now turn to the region between Thr359 and Tyr288 to examine the hypothesis that Thr359 can be a relay point that connects Ser299 with Tyr288.

3.2. Thr359–Tyr288

The region between Thr359 and Tyr288 is notable for its hydrophobic character [12] and, consequently, it may be hard to find waters that can form hydrogen-bonded chains. To illustrate this point, we first did a search on the crystal structure [12] to find receptive places for waters, based on the TW algorithm described in Computational methodology. The same algorithm was used, with a box of linear dimension 15 Å centered on the Thr359 CA atom. The grid spacing was reduced to 1 Å to provide finer resolution. The search method finds potential locations, based on the availability of space in the crystal structure, which would permit insertion of water(s). Fig. 5 shows the results of this scan with the "lattice lines" between two of the waters and around a third indicating that, around each explicitly shown water, there is room available for more than one water, but not enough room to place two waters. Thus, we may conclude that there is some room for a few waters that could be hydrogen-bonded to each other, and to residues, within this region of the crystal structure. The same scan procedure on the results of the MD around 3 ns (not shown) indicates that the situation is essentially the same, with some tendency that there is less room for water placement than in the crystal structure.

To examine the origin of water exclusion in the region between Thr359 and Tyr288, it is instructive to display the atoms in a cylinder whose axis is defined by Thr359 OG1 (the hydroxyl oxygen) and Tyr288 OH (the hydroxyl oxygen). The white line in Fig. 6 connects these atoms. Fig. 6 shows that the region between Thr359 and Tyr288 is quite hydrophobic; it is composed of residues Leu323, Leu326, Ile355, Ala356, Phe387 and Phe391, and the farnesyl tail of the heme a$_3$. Rotation of a stereo view of this figure shows that the farnesyl tail wraps around the cylinder axis and occupies a substantial fraction of the space between Thr392 and Tyr288. The waters that are associated with this region are hydrogen-bonded to backbone atoms of Leu326 and
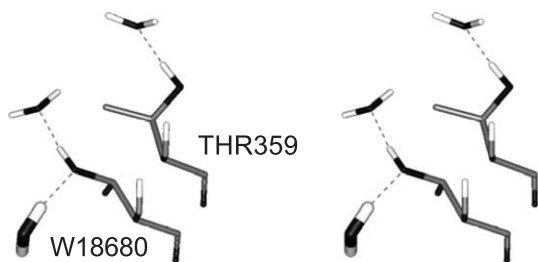

Fig. 4. Thr359 before and after OH rotation in stereo view. The hydroxyl group has rotated from a position pointing down (left-lower part of figure) to pointing up (right-higher part of figure). When pointing down to hydrogen bond to W18680, there can be a continuous hydrogen-bonded chain from Ser299 to Thr359. After Thr359 rotates, the water chain to Ser299 is disconnected, but now Thr359 is connected by a water hydrogen-bonded to the heme a$_3$ farnesyl hydroxyl (see Fig. 7).

Fig. 5. The region between Thr359 and Tyr288 with waters placed by our search algorithm in the crystal structure. All distances shown (in Å) are oxygen to oxygen. The displayed water with the "lattice work" surrounding it indicates that there is a great deal of space to place a water there, but two waters would not fit without some adjustment of the protein environment. The crystal structure has room for several waters to form a hydrogen-bonded chain that would span the hydroxyl groups of Thr359 and Tyr288.

Ala351, and the latter residue is quite far from the cylinder axis. By hydrogen bonding to backbone atoms, waters are not completely excluded from the region.

Even though the region is quite hydrophobic and snapshots show few waters, we still did an extensive channel search to verify the absence of water chains that span either Lys362-Tyr288 or Thr359-Tyr288. Two cylinders were defined: cylinder KY (TY) with Lys362 NZ and Tyr288 OH (Thr359 OG1 and Tyr288 OH) as the root and terminator, respectively, of the cylinder's axis. The cylinder radii are 10 Å. The easy criterion of hydrogen bonding was used (see Computational methodology) and data, taken every 0.1 ps, were analyzed for water chains with at least three waters. At no time during the approximately 1.5 ns of MD that were examined did any chain form. As an experiment, the definition of a hydrogen bond was revised to search for chains where the heavy atom distances were less than 4.5 Å, but even with this non-physical definition, no chains of three or more waters would span either of the two residues defining the TY and KY cylinders.

The lack of chain formation in this region makes it hard to understand how proton translocation in the K channel can occur. Of course, the MD time scale is quite short, and in this very hydrophobic region of the protein, it could be that filling of the region is just too slow. The TW procedure described in the methods is designed to alleviate the problem to a certain extent but it still is problematic. Thus,

Fig. 6. The region between Thr359 and Tyr288 showing the surrounding residues. The residues in a cylinder with axis defined by the white line joining the Thr359 and Tyr288 hydroxyls are all hydrophobic (Leu323, Leu326, Ile355, Ala356, Phe387, Phe391) and a good deal of the space between the two residues in-filled by the farnesyl tail of heme a3. (For colour see online version).
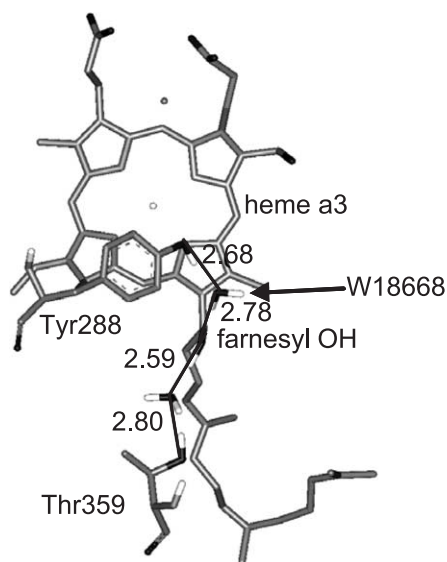
Fig. 7. Chain of waters that span Thr359 to Tyr288 via the heme a_3 farnesyl OH. Thr359 OH is pointing up to permit a water to bridge to the farnesyl OH. W18668 bridges the farnesyl OH and the Tyr288 OH, and does so very persistently. All distances are given in Å.

another approach was pursued when we noticed that a water hydrogen-bonded to the carbonyl, if moved about 3 Å closer to the Thr359 OG1 to hydrogen bond to it, would offer the possibility of forming a chain spanning Thr359 and Tyr288. That is, by restraining certain water(s) an attempt can be made to create a better environment for chain formation. This water was moved to hydrogen bonding distance of Thr359 over 100 ps by introducing a harmonic restraint with a continuously variable equilibrium position. Apparently there is sufficient room to do this maneuver since there were no difficulties in carrying out the restrained MD. Once the hydrogen bond was formed, we initiated two more MD simulations, each of 200-ps duration. One eliminated the harmonic restraint and the other maintained it to keep the water–Tyr359 hydrogen bond. After these simulations, the TY channel analysis was carried out as described above. The results were still negative; no chains of three or more hydrogen-bonded waters formed to span Thr359 and Tyr288.

The above negative results suggested that a residue, or residues, or part of the heme a_3 must be involved in proton transport in this region. Since the pathway here is so hydrophobic, the only possibility for hydrogen bonding to residues is the backbone amide and carbonyl functionalities and, for the heme a_3, the farnesyl hydroxyl. Thus, we broadened our water chain search procedure to include a chain that spans Thr359 and Tyr288 with the intervention of a residue or the farnesyl hydroxyl. The results of this enhanced channel search unequivocally point to the farnesyl hydroxyl as the important hydrogen bonding moiety for chain formation. Fig. 7 shows that chains can form leading from Thr359 to Tyr288 when the farnesyl hydroxyl is included in the definition of the chain. W18668 is hydrogen

bonding to the farnesyl O1B, acting as an acceptor, and to the Tyr288 OH, acting as a donor, and both hydrogen bonds are very strong. The solvation energy of the water is −20 kcal/mol, indicating its strong stabilization. Examination of the starting MD configuration from the X-ray structure [12] has the distances between the W18668 oxygen and the Tyr288 OH (farnesyl O1B) at 5.81 (4.93) Å. Thus, this water, which is a TW in Computational methodology designation, does not start out hydrogen-bonded to either the Tyr288 or the farnesyl hydroxyl. The interval between 1 and 1.4 ns shows movements that lead, by 1.4 ns, to W18668 in the hydrogen-bonded configuration displayed in Fig. 7. Remarkably, once there, it remains in this bridging position for the remaining 1.6 ns of the simulation. And, the fluctuations in its distances to both Tyr288 OH and farnesyl O1B remain on the scale of 1 Å for those 1.6 ns of simulation time. Once trapped, the solvation energy of W18668 remains around −20 kcal/mol, again indicating its stability at this site. The other water that bridges Thr359 OG to farnesyl O1B is less stable relative to W18668. From the beginning of the simulation, it takes about 1.2 ns before a water or waters move into position to bridge Thr359 and farnesyl O1B. Once this bridge forms, it persists on the scale of 400 ps. Usually a bridging water is present at any time. There are periods with two hydrogen-bonded waters between Thr359 and O1B. In the 1.6 ns after formation of Thr359 farnesyl O1B bridges, there is one 200-ps interval with two hydrogen-bonded waters bridging them. These features indicate the sparseness and lack of stability of waters between Thr359 and O1B. Indeed, among the approximately 2 ns/0.1 ps=20,000 configurations examined for hydrogen-bonded water chains, we found only one where Ser299 could be thought of as continuously linked to the farnesyl O1B. Fig. 8 shows this connection. The link between W8827 and the Thr359 hydroxyl is not displayed as a hydrogen bond since the O–H–O angle is around 45 ° even though the distance is 3.27 Å.
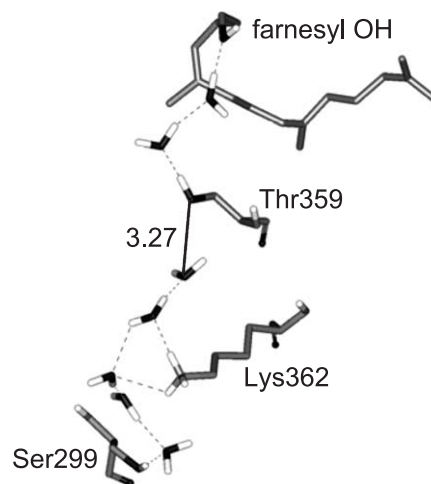

Fig. 8. A chain of hydrogen-bonded waters and residues that spans Ser299 to the farnesyl hydroxyl. The water "hydrogen-bonded" to Thr359 from below has a (non-hydrogen bonding) 45 ° angle.

3.3. Tyr288–a₃Fe/Cu_B

The last part of the K channel connects Tyr288 to the binuclear center. What is of interest is the pattern of waters that are present in the vicinity of Tyr288, the heme a_3 Fe and Cu_B. The configuration displayed in Fig. 9 shows the hydrogen-bonded pattern of Tyr288 OH–W18618–W18402–W5005. Furthermore, the W18402 Fe (Cu_B) distance is 2.66 Å (2.78 Å), the W5005 Cu_B distance is 2.27 Å, and W5005 hydrogen bonds to the heme a_3 D propionate. The W18402 solvation energy is −30 kcal/mol, the large value being indicative of its ligation to the Fe as well as the hydrogen bond to W5005. The W5005 solvation energy is −16 kcal/mol, the smaller value relative to W18402 reflecting in part the smaller and more diffuse charge associated with Cu_B and its ligands (see Computational methodology). The snapshot for the figure is around 3 ns; aspects of the structure are not present until around this time. The W5005 only enters the binuclear region around 2 ns and, at various times, it associates with Tyr288, His333, His334, the heme a_3 D propionate and Cu_B. Thus, once it is trapped in the site, it still displays considerable mobility. The W18402 appears around 1.5 ns and associates with the same set of atoms as W5005 before taking up the Fe and Cu_B bridging role shown in Fig. 9. The W18668 also enters the binuclear site around 1.5 ns and then it assumes the bridging role between the farnesyl hydroxyl and the Tyr288 hydroxyl, as discussed in the previous section. In Fig. 9, where the farnesyl hydroxyl is hydrogen-bonded to the Tyr288 hydroxyl, W18668 is displaced from the more direct bridging configurations, as shown in Fig. 7, where the farnesyl hydroxyl–Tyr288 hydroxyl distance is larger. Nevertheless, W18668 is still quite close to the farnesyl O1B (3.8 Å).
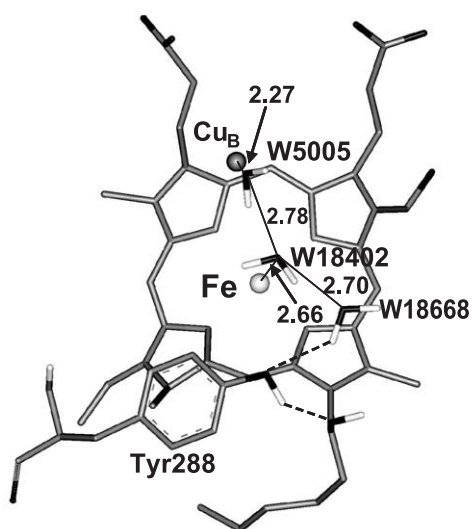

Fig. 9. The water structure spanning Tyr288 and the binuclear center with the heme a_3 displayed. The phenolic oxygen of Tyr288 is hydrogen-bonded to a chain of three waters, and W18402 ligates to the heme a_3 Fe and W5005 ligates to Cu_B. All distances are given in Å.

4. Discussion

The discussion will be organized to mirror the three regions of the K channel introduced in Results. In the crystal structure, a hydrogen-bonded water is found to connect Ser299 and Lys362 [12]. Crystallography can reveal the presence of stable waters, versus labile waters, though it is not straightforward to make these notions quantitative. The simulation finds that Ser299 and Lys362 are bridged by persistent water, according to our definition of a greater than 100-ps residence time. In Figs. 2 and 3, which are snapshots taken from configurations around the 3-ns end point of our simulation, W8827 is persistent for at least 100 ps. Examination of the trajectory for earlier times shows that eventually (about 400 ps earlier) W8827 is no longer bridging; however, it is replaced by another bridging water. This water is first present around 1.5 ns and persists forward in time for about 1.3 ns before it becomes replaced by W8827. Thus, we may conclude that most of the time there is a bridging water present, and it can persist on the nanosecond time scale. The solvation energy of W8827 (cf. Table 2) is consistent with stability on the hundreds of picosecond time scale as found here.

Electrostatic calculations had suggested that Lys362 is deprotonated over a large pH range but, in addition to the usual uncertainties of these calculations, where assumptions about the prevailing dielectric constant in the interior of a protein must be made, waters were not included in the calculation [42]. In a medium of dielectric constant 4, as may be appropriate to a hydrophobic region in a protein, a lysine's pK_a~10 could be substantially reduced to suggest that it could be deprotonated at pH~7. However, the presence of hydrogen-bonded waters, and we found that there are approximately three on average around (protonated) Lys362, will certainly drive the pK_a back toward the solution value. Indeed, a pK_a that is essentially a solvation phenomenon measure relies not only on the presence of dipoles but on their ability to reorient. That is, for a given density of dipoles, as the ability for them to reorient increases their ability to solvate and stabilize a charge increases. The combination of persistent and mobile waters found in the vicinity of Lys362 in the simulation suggests that it should be protonated. That Lys362 is protonated around pH 7 has been inferred by the kinetic flash-flow data of Branden et al. [41].

The side chain of Lys362 has been proposed to be part of a charge compensation mechanism by reorienting in response to charge transfer events in the binuclear center [17,41]. Since our simulation has been carried out to model the fully reduced enzyme, we cannot comment on this scenario. However, for the fixed charge state of the simulation, the distances presented in Table 1 certainly show that the side chain of Lys362 is quite restricted in its movement. The approximately 1-Å excursions in the Ser299 CA–Lys362 NZ and Lys362 NZ–Thr359 CA distances (see Table 1) over the 3-ns simulation do not support a rotation of

the lysine side chain. However, the simulation does suggest an alternative possibility whereby the Thr359 side chain undergoes a rotation in conjunction with the formation of differing patterns of hydrogen-bonded waters. As displayed in Fig. 4, when the Thr359 hydroxyl group points downward, water chains that connect with the Ser299 hydroxyl form. These chains are not present all the time, of course, but there are a sufficient number of waters in this region of the protein to occasionally form these spanning chains. Note that the chain displayed in Fig. 2 has five hydrogen bonds that are simultaneously present to connect the four waters and two residues. When the Thr359 hydroxyl rotates to point upward, it is more difficult to form chains to connect to Ser299.

The importance of Thr359 in *R. sphaeroides* has been demonstrated by mutating it to alanine [25], since this mutation leads to a reduction in activity to 20–35% of that in the wild type. At the same time, the optical and resonance Raman experiments show that the structure of the heme binuclear center is not changed by the mutation. An analysis of the proton-pumping capability of the mutant [43] indicates a normal efficiency, which also suggests that the loss of steady state activity is not attributable to modification of the binuclear center. The conclusion reached by Hosler et al. [25] that Thr359 plays a role in facilitating proton translocation to the binuclear center is well supported by the results of our simulation. When higher-resolution structures of CCO become available, it will be of great interest to compare the pattern of hydrogen-bonded waters around Thr359 with those suggested by the simulation.

Once the Thr359 hydroxyl has rotated, breaking the connection with Ser299, it is in better position to hydrogen bond to a water that can then hydrogen bond to the heme a_3 farnesyl hydroxyl. The extensive search that we carried out for direct hydrogen-bonded water chains spanning Thr359 and Tyr288 showed that over the entire MD simulation time, there are no such chains. In the *R. Sphaeroides* crystal structure [12], the region between Thr359 and Tyr288 does have room for a few water molecules, as shown in Fig. 5. Our search algorithm uses a combination of geometric (from van der Waals repulsion) and energetic (from electrostatics) criteria to find likely places for waters. The "lattice lines" around some of the waters in Fig. 5 indicate that those displayed waters have additional room to be placed, though not so much that two waters could occupy the space where one water is displayed. As the simulation progresses, this region does not gain waters; if anything, the density of water slightly decreases, and this may be a consequence of a slight reduction in volume from the "extra" space found in the crystal structure. In any case, this region of the protein is clearly effective in excluding water. Fig. 6 shows that this region is hydrophobic, partly from the residues that occupy the space in a cylinder whose axis is defined by the white line from the Thr359 hydroxyl to the Tyr288 hydroxyl, and partly from the heme a_3 farnesyl tail that wraps around the

cylinder axis. That leaves the farnesyl hydroxyl as a polar group in this region of the protein. These features stimulated our search for water chains from the rotated Thr359 hydroxyl to "use" the farnesyl hydroxyl as a protonatable group on the way to Tyr288.

The structure in Fig. 7 shows how Thr359 and Tyr288 can be connected with one water bridging the Thr359 and farnesyl hydroxyls and another water bridging the farnesyl and Tyr288 hydroxyls. The potential role of the farnesyl hydroxyl in providing a protonatable group for O_2 splitting in oxidase has been discussed by Wikström [7] and Blomberg et al. [26,44]. They suggested that an extra proton provided by protonation of the farnesyl hydroxyl can be transferred to the Tyr288 hydroxyl group and, in this fashion, be available to the binuclear center for the O_2 splitting step. The additional proton is required in their reaction scheme to provide a low barrier for O–O bond cleavage; in its absence, the barriers are calculated to be much too high. In our simulations, the farnesyl hydroxyl is sometimes too far from the Tyr288 hydroxyl (4–5-Å oxygen–oxygen distance) to form a hydrogen bond but, in those cases, W18668 bridges them, as is the case in Fig. 7. That would also provide the hydrogen bond (from W18668 to the Tyr288 hydroxyl) and, with this water bridging to the farnesyl hydroxyl, also provide a path for conduction of the excess proton. In many other configurations (not shown), the Tyr288 hydroxyl to farnesyl hydroxyl oxygen–oxygen distance is around 2.7 Å, as in the crystal structure (2.87 Å), and then there is the direct farnesyl–tyrosine hydrogen bond envisaged in their mechanism. In these situations, the stable W18668 is still hydrogen-bonded to at least the Tyr288 hydroxyl and, often, also to the farnesyl hydroxyl. The solvation energy of about −20 kcal/mol is the same in both situations and serves to confirm the stability of this water. The presence of a hydrogen-bonded water either as a bridge between the farnesyl and the Tyr288 hydroxyls or as a hydrogen bonding partner of one or both of them may be significant in modifying the energetics relevant to the reaction mechanism for oxygen chemistry. The water can stabilize protonation of the farnesyl hydroxyl, in addition to the Blomberg et al. [26,44] stabilization mechanism of resonance stabilization from the π-system of the heme a_3 ring. To summarize, in support of their mechanism, delivery of a K-pathway proton can be accomplished since, as shown in Fig. 7, there can be continuous chains of waters spanning the hydroxyls of Thr359 to Tyr288, when the only polar group in that region, the farnesyl hydroxyl, is included in the definition of a chain.

We have emphasized the Thr359 hydroxyl rotation as a means of providing water chains that can span Thr359 to Tyr288. We did find 1 out of 20,000 configurations in the 2-ns time interval between 1.2 and 3.2 ns where water/residue/farnesyl chains that could support a direct connection between Ser299 and Tyr288 actually formed, though, as shown in Fig. 8, the water to Thr359 bond angle is not correct for a hydrogen bond. The interval between successive

K channel output data is 0.1 ps. This is a short enough time interval to be confident that the picture could only change qualitatively if the output interval were shortened. Thus, it seems that the rotation of Thr359 is important to providing configurations for connecting Ser299 and Tyr288. However, it should be realized that the MD time scale is certainly short. A factor of 1/20,000 roughly corresponds to an activation energy of 5 kcal/mol and, with an assumed Arrhenius pre-factor of 10^{13} s^{-1}, the event time scale would be around 0.5 ns. Thus, on a microsecond time scale there would be the possibility of chains forming without the requirement of a Thr359 rotation. Obviously, there is an energy cost for the Thr359 hydroxyl group rotation and its (free) energy barrier could certainly be on the scale of 5 kcal/mol. Of course, both mechanisms can coexist, and an intensified experimental focus on the role of Thr359 may provide discrimination between them. The substantial decrease in activity upon Thr359Ala mutation [25] does support the Thr359 switching mechanism advanced here.

In the region around the binuclear center where the oxygen chemistry takes place, the crystal structure of *R. sphaeroides* [12] reveals a critical role for the heme a$_3$ Fe, the Cu$_B$ and a number of residues including the Tyr288 and His284. The crystal structures of the bovine [14] and *Paracoccus* [15] enzymes show that the tyrosine and histidine corresponding to Tyr288 and His284 in *R. sphaeroides* are covalently linked, while in the *R. sphaeroides* structure this cross-link is not so evident; nevertheless, we have assumed that it is in the simulation. The presence of water(s) in the binuclear site is essential to the postulated mechanisms of O–O bond cleavage. The X-ray structure suggests a water (or hydroxide) as the fourth ligand of Cu$_B$, and another possibly around the Tyr288 hydroxyl or its CB carbon atom. Data from EXAFS [45] suggest a water ligates to a Cu$_B$. There is inferential evidence from resonance Raman spectroscopy of the presence of water in the binuclear site [46,47]. Kinetic studies [48] show that water (and hydroxide) is intimately involved in the binuclear site. Extensive quantum chemical modeling studies of the O–O bond cleavage starting from the heme a$_3$ Fe(III)–Cu$_B$(I) mixed-valence oxidation state initially suggested a role for one water [26,49] and, later, for two waters [44]. In this latter study, one water molecule is associated with bridging O$_2$ and tyrosine and another bridges the farnesyl and tyrosine hydroxyls. In mechanistic proposals of oxygen reduction, O$_2$ initially binds to the Fe to form an oxy complex with the Cu$_B$ close to the distal oxygen of O$_2$. A role of the K channel is to provide a proton to the binuclear site [17] that may be supplied by protonation of the farnesyl hydroxyl. The so-delivered proton is transferred to the tyrosine and then to O$_2$. Other proposals use one water either associated with the tyrosine or Cu$_B$ or a protonated water molecule directly associated with O$_2$ [50]. These mechanisms have the common features that an "extra" proton is involved, and the farnesyl hydroxyl is viewed as a site of protonation that can provide a proton to the cross-linked tyrosine. Once the proton is delivered to the tyrosine, it can be used in O$_2$ reduction with the involvement of one or two waters.

Our simulations are carried out for a fully reduced oxidation state and, therefore, we cannot examine changes in the binuclear site geometry engendered by the redox chemistry that is of course required for O$_2$ reduction. Also, oxygen is not present. Since the reaction can be initiated from either a fully reduced or mixed valence state, our simulations can provide information on the presence, number and arrangement of water in the binuclear site. As shown in Fig. 9, the three waters found are well positioned to support the O$_2$ reduction mechanistic suggestions. The configuration displayed in Fig. 9 has W18668 hydrogen-bonded to the Tyr288 hydroxyl. It does so very persistently since, once it becomes hydrogen-bonded (around 1.4 ns), it remains so for the remainder of the 1.6-ns simulation. It is hard to find other waters with such stability in the simulation. The solvation energy of this water is −20 kcal/mol, and while there are other waters that are more solvated (such as those ligated to metals), this solvation energy correlates well with persistence. Thus, the MD supports a special role for water hydrogen bonding to the cross-linked tyrosine. From our finding that Ser299 and Tyr288 are in fact connected by a hydrogen-bonded water chain via the farnesyl hydroxyl, we can also support the suggestion that the farnesyl hydroxyl could be protonated, and that proton made available to Tyr288 through a mutually hydrogen-bonded water such as W18668. In Fig. 9, the W18668 distance is just beyond hydrogen bonding distance; however, as noted in Results, most other snapshots show W18668 in a more bridging configuration between the farnesyl and Tyr288 hydroxyls, since the farnesyl O1B to Tyr288 OH distance does fluctuate between the crystal structure separation of 2.87 Å and around 4–5 Å.

The W18402 in Fig. 9 is 2.66 Å from the heme a$_3$ Fe and 4.2 Å from Cu$_B$. The W5005 Cu$_B$ distance is 2.27 Å; W5005 may be acting like the *product* water of the O$_2$ reduction. It is hydrogen-bonded to W18402 that, in turn, is hydrogen-bonded to W18668. Thus, we may interpret our simulation result as a "two-water" mechanism, with the third water (W5005) that we find in the binuclear site the product water. Once in the binuclear site (after about 2 ns of simulation time), W5005 stays there for the remaining simulation time; but it exhibits quite a bit of mobility, sometimes hydrogen bonding to His333, His334, and even Tyr288, as well as the heme a$_3$ D propionate and Cu$_B$. W18402 is also quite mobile even after it enters the binuclear site around 1.5 ns of simulation time. It also hydrogen bonds with His333, His334 and Tyr288 and Cu$_B$, before "settling" on a bifurcated coordination with the heme a$_3$ Fe and Cu$_B$. The distance between W18402 and the Tyr288 OH is around 4 Å; thus, it does not require much movement of this water to also hydrogen bond to Tyr288.

5. Concluding remarks

The sparseness of water found in the crystallographic study of CcO from *R. sphaeroides* in the region of the K channel stimulated a careful search for water pathways that we have carried out by MD simulation. By using a large number of waters of solvation and by initially inserting waters at favorable sites within the protein, the 3 ns of simulation time did provide enough time for the formation of water chains. The methods we have developed to examine the possible formation of water trees on a short (0.1 ps) time scale enhances the probability of finding "rare" configurations, even on the relatively short MD simulation time scale. Since, within a protein, the formation of simultaneously hydrogen-bonded waters becomes increasingly improbable as the number of hydrogen-bonded waters increases, other things being equal, it is imperative to be able to search on a short time scale.

Since Ser299 is essentially solvent-exposed and Lys362 was protonated for the simulation, the formation of water chains in this region should not be difficult, and this is what was found. Interestingly, the Lys362 side chain was found to be quite stable. Instead of it rotating, the simulation supports the possibility of the Thr359 side chain as a pivot point that, when it is pointing down, provides hydrogen-bonded chains connecting to Ser299 and, when it is pointing up, breaking this connection and, instead, provides water chains to Tyr288. The determination that Thr359 is important to enzyme function, as found by mutational studies [25], and the mechanistic suggestions presented here based on the simulation results, suggest that more attention should be devoted to the residue and its vicinity. In particular, experimental and computational investigations that probe the acidity of Thr359 and elucidate its proton translocation ability would be helpful in defining its function in CcO.

The region between Thr359 and Tyr288 is quite hydrophobic and our main conclusion is that the only way to form water chains is with the use of the heme a_3 farnesyl hydroxyl. Once this hydroxyl is included in the search scheme, the possibility of a proton conduction pathway from Thr359 to Tyr288 is evident. Thus, we consider that the farnesyl hydroxyl could play a key role in the K channel function. The insights from quantum chemical studies also identify this hydroxyl as key, based on a proposed mechanism for O_2 bond splitting at the binuclear site. The simulation results in the Tyr288 to binuclear site region also dovetail very nicely with mechanistic suggestions for O_2 reduction [26,44,49]. Indeed, the pattern of three waters found around Tyr288, Fe and Cu_B, their persistence, and their solvation energies, arising from hydrogen bonding to residues, other waters and ligation to metals, suggests that the binuclear center is designed to function with specific waters. While the solvation energies that are evaluated are not free energies, it is still instructive that the typical persistent water energies are around -18 kcal/mol, and are comparable to the water-in-water solvation energy. The implication for CcO is that the waters are not so solvated as to be immobile yet are sufficiently solvated to be transiently available for chemical purposes, such as for O_2 reduction.

The simulation results we have presented are for the fully reduced state of the enzyme. Clearly, it would be quite interesting to study other oxidation states, and the structural changes engendered by changes in oxidation state, corresponding to successive redox stages of the enzyme.

Acknowledgement

References

[1] M.K.F. Wikström, Proton pump coupled to cytochrome *c* oxidase in mitochondria, Nature 266 (1977) 271–273.

[2] B.G. Malmström, Cytochrome *c* oxidase as a redox-linked proton pump, Chem. Rev. 90 (1990) 1247–1260.

[3] B.G. Malmström, Vectorial chemistry in bioenergetics: cytochrome *c* oxidase as a redox-linked proton pump, Acc. Chem. Res. 26 (1993) 332.

[4] S. Papa, N. Capitanio, G. Villani, G. Capitanio, A. Bizzoca, L.L. Palese, V. Carlino, E. De Nitto, Cooperative coupling and role of heme alpha in the proton pump of heme-copper oxidases, Biochimie 80 (1998) 821–836.

[5] S. Ferguson-Miller, G.T. Babcock, Heme/copper terminal oxidases, Chem. Rev. 96 (1996) 2889.

[6] See articles on cytochrome *c* oxidase in, Biochim. Biophys. Acta 1458 (2000).

[7] M. Wikström, Mechanism of proton translocation by cytochrome *c* oxidase: a new four-stroke histidine cycle, Biochim. Biophys. Acta 1458 (2000) 188–198.

[8] P. Brzezinski, G. Larsson, Redox-driven proton pumping by heme-copper oxidases, Biochim. Biophys. Acta 1605 (2003) 1–13.

[9] J.F. Nagle, S. Tristam-Nagle, Hydrogen bonded chain mechanisms for proton conduction and proton pumping, J. Membr. Biol. 74 (1983) 1–14.

[10] N. Agmon, The grotthuss mechanism, Chem. Phys. Lett. 244 (1995) 456.

[11] T. Tsukihara, H. Aoyama, E. Yamashita, T. Tomizaki, H. Yamaguchi, K. Shinzawa-Itoh, R. Nakashima, R. Yaono, S. Yoshikawa, The whole structure of the 13-subunit oxidized cytochrome *c* oxidase at 2.8 angstrom, Science 272 (1996) 1136–1144.

[12] M. Svensson-Ek, J. Abramson, G. Larsson, S. Tornroth, P. Brzezinski, S. Iwata, The X-ray crystal structures of wild-type and EQ(I-286) mutant cytochrome *c* oxidases from *Rhodobacter sphaeroides*, J. Mol. Biol. 321 (2002) 329–339.

[13] I. Hofacker, K. Schulten, Oxygen and proton pathways in cytochrome *c* oxidase, PROTEINS structure, Funct. Genet. 30 (1998) 100–107.

[14] S. Yoshikawa, K. Shinzawa-Itoh, R. Nakashima, R. Yaono, E. Yamashita, N. Inoue, M. Yao, M.J. Fei, C.P. Libeu, T. Mizushima, H. Yamaguchi, T. Tomizaki, T. Tsukihara, Redox-coupled crystal structural changes in bovine heart cytochrome *c* oxidase, Science 280 (1998) 1723–1729.

[15] C. Ostermeier, A. Harrenga, U. Ermler, H. Michel, Structure at 2.7 angstrom resolution of the *Paracoccus denitrificans* two-subunit cytochrome *c* oxidase complexed with an antibody F-V fragment, Proc. Natl. Acad. Sci. U. S. A. 94 (1997) 10547–10553.

[16] K.M. McCauley, J.M. Vrtis, J. Dupont, W.A. van der Donk, Insights into the functional role of the tyrosine-histidine linkage in cytochrome c oxidase, J. Am. Chem. Soc. 122 (2000) 2403–2404.

[17] M. Branden, F. Tomson, R.B. Gennis, P. Brzezinski, The entry point of the K-proton-transfer pathway in cytochrome c oxidase, Biochemistry 41 (2002) 10794–10798.

[18] F.L. Tomson, J.E. Morgan, G.P. Gu, B. Barquera, T.V. Vygodina, R.B. Gennis, Substitutions for glutamate 101 in subunit II of cytochrome c oxidase from Rhodobacter sphaeroides result in blocking the proton-conducting K-channel, Biochemistry 42 (2003) 1711–1717.

[19] R.I. Cukier, Theory and simulation of proton-coupled electron transfer, hydrogen-atom transfer, and proton translocation in proteins, Biochim. Biophys. Acta 1655 (2004) 37–44.

[20] R.I. Cukier, Quantum molecular dynamics of proton transfer in cytochrome c oxidase, Biochim. Biophys. Acta 1656 (2004) 189–202.

[21] R.I. Cukier, S.A. Seibold, Molecular dynamics simulations of prostaglandin endoperoxide II synthase-1: role of water and the mechanism of compound I formation from hydrogen peroxide, J. Phys. Chem., B 106 (2002) 12031–12044.

[22] H. Michel, Cytochrome c oxidase: catalytic cycle and mechanisms of proton pumping—a discussion, Biochemistry 38 (1997) 15129–15140.

[23] A.S. Pawate, J. Morgan, A. Namslauer, D. Mills, P. Brzezinski, S. Ferguson-Miller, R.B. Gennis, A mutation in subunit I of cytochrome oxidase from Rhodobacter sphaeroides results in an increase in steady-state activity but completely eliminates proton pumping, Biochemistry 41 (2002) 13417–13423.

[24] S. Iwata, C. Ostermeier, B. Ludwig, H. Michel, Structure at 2.8-angstrom resolution of cytochrome-C-oxidase from Paracoccus denitrificans, Nature 376 (1995) 660–669.

[25] J.P. Hosler, J.P. Shapleigh, D.H. Mitchell, Y. Kim, M.A. Pressler, C. Georgiou, G.T. Babcock, J.O. Alben, S. Ferguson-Miller, R.B. Gennis, Polar residues in helix VIII of subunit I of cytochrome c oxidase influence the activity and the structure of the active site, Biochemistry 35 (1996) 10776–10783.

[26] M.R.A. Blomberg, P.E.M. Siegbahn, G.T. Babcock, M. Wikstrom, O–O bond splitting mechanism in cytochrome oxidase, J. Inorg. Biochem. 80 (2000) 261–269.

[27] S. Riistama, G. Hummer, A. Puustinen, R.B. Dyer, W.H. Woodruff, M. Wikström, Bound water in the proton translocation mechanism of the haem-copper oxidases, FEBS Lett. 414 (1997) 275–280.

[28] R. Pomès, G. Hummer, M. Wikström, Structure and dynamics of a proton shuttle in cytochrome c oxidase, Biochim. Biophys. Acta 1365 (1998) 255–260.

[29] D.M. Medvedev, I. Daizadeh, A.A. Stuchebrukhov, Electron transfer tunneling pathways in bovine heart cytochrome c oxidase, J. Am. Chem. Soc. 122 (2000) 6571–6582.

[30] X. Zheng, D.M. Medvedev, J. Swanson, A.A. Stuchebrukhov, Computer simulation of water in cytochrome c oxidase, Biochim. Biophys. Acta 1557 (2003) 99–107.

[31] M. Wikström, M.I. Verkhovsky, G. Hummer, Water-gated mechanism of proton translocation by cytochrome c oxidase, Biochim. Biophys. Acta 1604 (2003) 61–65.

[32] D.M. Popovic, A.A. Stuchebrukhov, Electrostatic study of the proton pumping mechanism in bovine heart cytochrome c oxidase, J. Am. Chem. Soc. 126 (2004) 1858–1871.

[33] A.A. Stuchebrukhov, Electron transfer reactions coupled to proton translocation: cytochrome oxidase, proton pumps, and biological energy transduction, J. Theor. Comp. Chem. 2 (2003) 91–118.

[34] W.F. van Gunsteren, H.J.C. Berendsen, GROMOS Manual, University of Groningen, Groningen, 1987.

[35] R.W. Hockney, J.W. Eastwood, Computer Simulation Using Particles, McGraw-Hill, New York, 1981.

[36] M.P. Allen, D.J. Tildesley, Computer Simulation of Liquids, Clarendon Press, Oxford, 1987.

[37] J.P. Ryckaert, G. Ciccotti, H.J.C. Berendsen, Numerical-integration of Cartesian equations of motion of a system with constraints—molecular dynamics of N-alkanes, J. Comput. Phys. 23 (1977) 327–341.

[38] H.H.C. Berendsen, J.P.M. Postma, W.F. Gunsteren, A. DiNola, J.R. Haak, Molecular dynamics with coupling to an external bath, J. Chem. Phys. 81 (1984) 3684–3690.

[39] Coordinates kindly provided by Professor S. Ferguson-Miller.

[40] E.I. Solomon, U.M. Sundaram, T.E. Machonkin, Multicopper oxidases and oxygenases, Chem. Rev. 96 (1996) 2563–2605.

[41] M. Branden, H. Sigurdson, A. Namslauer, R.B. Gennis, P. Adelroth, P. Brzezinski, On the role of the K-proton transfer pathway in cytochrome c oxidase, Proc. Natl. Acad. Sci. U. S. A. 98 (2001) 5013–5018.

[42] A. Kannt, C.R.D. Lancaster, H. Michel, The coupling of electron transfer and proton translocation: electrostatic calculations on Paracoccus denitrificans cytochrome c oxidase, Biophys. J. 74 (1998) 708–721.

[43] J.R. Fetter, J. Qian, J. Shapleigh, J.W. Thomas, A. Garcia-Horsman, E. Schmidt, J. Hosler, G.T. Babcock, R.B. Gennis, S. Ferguson-Miller, Possible Proton Relay Pathways in Cytochrome-C-Oxidase, Proc. Natl. Acad. Sci. U.S.A. 92 (1995) 1604–1608.

[44] M.R.A. Blomberg, P.E.M. Siegbahn, M. Wikstrom, Metal-bridging mechanism for O–O bond cleavage in cytochrome c oxidase, Inorg. Chem. 42 (2003) 5231–5243.

[45] M. Ralle, M.L. Verkhovskaya, J.E. Morgan, M.I. Verkhovsky, M. Wikstrom, N.J. Blackburn, Coordination of Cu-B in reduced and CO-liganded states of cytochrome bo(3) from Escherichia coli, is chloride ion a cofactor? Biochemistry 38 (1999) 7185–7194.

[46] D.A. Proshlyakov, T. Ogura, K. Shinzawa-Itoh, S. Yoshikawa, T. Kitagawa, Resonance Raman/absorption characterization of the oxo intermediates of cytochrome c oxidase generated in its reaction with hydrogen peroxide: pH and H2O2 concentration dependence, Biochemistry 35 (1996) 8580–8586.

[47] M. Aki, T. Ogura, K. Shinzawa-Itoh, S. Yoshikawa, T. Kitagawa, A new measurement system for UV resonance Raman spectra of large proteins and its application to cytochrome c oxidase, J. Phys. Chem., B 104 (2000) 10765–10774.

[48] M. Branden, A. Namslauer, O. Hansson, R. Aasa, P. Brzezinski, Water–hydroxide exchange reactions at the catalytic site of heme-copper oxidases, Biochemistry 42 (2003) 13178–13184.

[49] M.R.A. Blomberg, P.E.M. Siegbahn, G.T. Babcock, M. Wikstrom, Modeling cytochrome oxidase: a quantum chemical study of the O–O bond cleavage mechanism, J. Am. Chem. Soc. 122 (2000) 12848–12858.

[50] Y. Yoshioka, H. Kawai, K. Yamaguchi, Theoretical study of role of H2O molecule on initial stage of reduction of O-2 molecule in active site of cytochrome c oxidase, Chem. Phys. Lett. 374 (2003) 45–52.